Determination of interfacial transition zone in cementitious materials by dynamic displacement

Huang Hsing Pan [1]; Kun-Sheng Liao [2]

Summary

An alternative method by using electronic speckle pattern interferometer (ESPI) to determine the range of interfacial transition zone is presented. ESPI method is capable of capturing dynamic displacements up to a precision of 10nm. In-plane displacements subjected to a continuous external loading from 0 to $0.7f_c'$ are observed near single aggregate. From the change of normalized displacement, a criterion to decide the scope of ITZ is proposed and also verified by SEM. Results show that the turning point in displacement diagram indicates the boundary of ITZ or the position of a crack. Based on normalized in-plane displacements, the range of ITZ near the top, bottom, left and right observing points is 80μm, 90μm, 80μm and 60μm respectively. The applied stress does not affect the determination of ITZ according to ESPI measurement before the specimen failed. A side effect to interpret the stress-strain behavior of cementitious materials is also discussed.

Keywords

interfacial transition zone, concrete, dynamic displacement, ESPI.

Theme

analysis – action engineering – conventional loads – materials - concrete

1. Introduction

Interfacial transition zone (ITZ) developing around the aggregate is a weak layer that dominates the strength of concrete. The microstructure of ITZ in cementitious material depends on cement paste, pozzolanic materials, the aggregate and the age [1]. Many microscopic techniques were selected to investigate the compositions and microscopic structure of ITZ such as scanning electron microscopy (SEM) [2-6], backscattered electron images (BSE) [7], environmental scanning electron microscopy (ESEM) and optical microscopy (OM) [8-9]. Other methods with respect to X-ray diffraction test [4,10], mercury intrusion porosimetry (MIP) [9,11] and micro-indentation test [5,12] were also used to evaluate material properties of ITZ. Most of them distinguish the realm of ITZ by exploiting the image, the porous and loose characteristic in ITZ. Some researchers discussed the microstructural feature, stress-strain relation and microcracks of ITZ subjected to temperatures [13-15]. Although SEM, OM, X-ray diffraction, MIP and micro-indentation tests are adequate to determine the range of ITZ, these methods can only observe a point or tiny part inside the sample with requiring sophisticated manufacturing processes. Meanwhile, to maintain the original state of the material is difficult as using present measurement techniques.

As an alternative, we use dynamic displacements measured by ESPI to determine the range of ITZ. ESPI method different from SEM belonging to a non-contact measurement has been adopted to analyze the strain in thin wall cylinders [16] and the displacement of sandwich plates [17]. In this study, a judgment of interfacial transition zone lying between the binder matrix and one coarse aggregate is discussed. Displacements of the specimen subjected to external loadings were captured by ESPI, and these dynamic displacements are suitable for estimating the scope of ITZ.

[1] Professor, Dept. of Civil Engineering, Kaohsiung Uni. of Applied Sciences, Kaohsiung/Taiwan pam@cc.kuas.edu.tw

[2] Grad. student, Dept. of Civil Eng., Kaohsiung Uni. of Applied Sciences, Kaohsiung/Taiwan x917052x@yahoo.com.tw

2. Materials and Measurement

2.1 Materials

A cubic specimen with a dimension of 50×50×50mm contains binder matrix and one sand stone (aggregate) located at the center of the specimen (figure 1). The binder is composed of 80% Type I Portland cement and 20% fly ash in weight, with a 0.6 water-to-binder ratio (w/b). The particle size of sand stone is about 13 ~ 18mm, with a density of 2.68 kg/cm^3 and absorption of 1.24%.

Specimens were cast into steel moulds and removed from the moulds after 24 hours, then cured in water till one day before external loadings applied onto them. The material age is of 56 days in the test. The continuous displacements of specimen subjected to external loadings from 0 to 0.7 f_c' were measured by ESPI simultaneously. We focused on the displacements of an investigated area (20×20mm) in the specimen (figure 2), and discussed ITZ near four observing points as marked by T (top), B (bottom), L (left) and R (right) respectively.

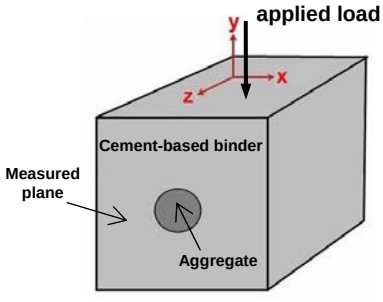

Figure 1: the schematic specimen (50×50×50mm)

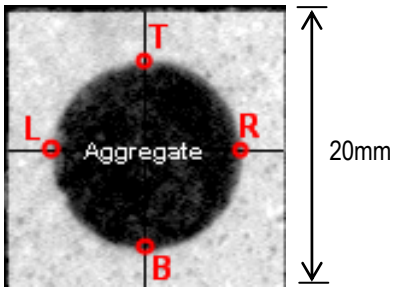

Figure 2: investigated area of displacement (20×20mm)

2.2 Measurement

Specimens were tested by means of a material testing system (MTS 810) with a compressive strain rate 5×10^{-4}/sec. Dynamic displacements of the specimen were measured by green-light ESPI with a wavelength of 532μm. The displacements in x-y plane (measured plane, figure 1), or so-called in-plane displacement (U-field displacement), were obtained by calculating speckle interfere pattern observed by ESPI (figure 3). We captured U-field speckle interfere pattern per 0.1 f_c' until the loading reached 0.7 f_c'. By using a charge coupled device (CCD) and four steps phase shifting procedures, the displacement converted from image of U-field interfere pattern displays a precision with 10nm per contour line. The position-displacement coordinate transformed from a phase unwrap diagram shows the position represented by (*x*, *y*) and a displacement with the value of *z* (figure 4).

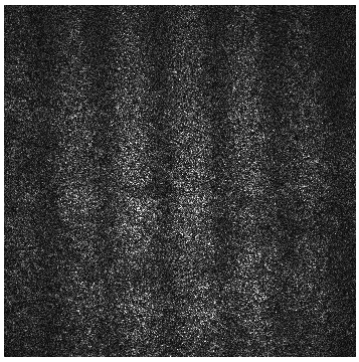

Figure 3: U-field interfere pattern

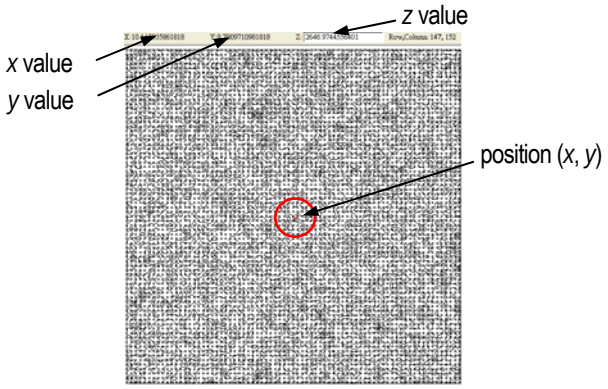

Figure 4: position-displacement coordinate

To determine ITZ, we captured the displacements within 170μm region away from the surface of aggregate. For example, an observing point marked a circle is at the left side of aggregate (figure 5), and three neighboring positions is located on this observing point with a distance of 60μm (figure 6), where L1, L2 and L3 are the points on the surface of aggregate. We measured dynamic displacements along the line 10μm each vertical to the surface of aggregate.

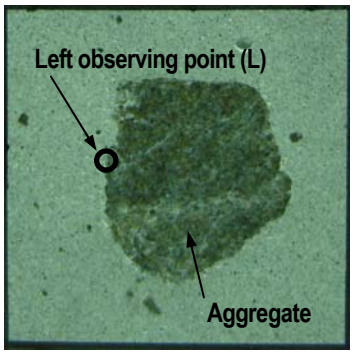

Figure 5: observing point

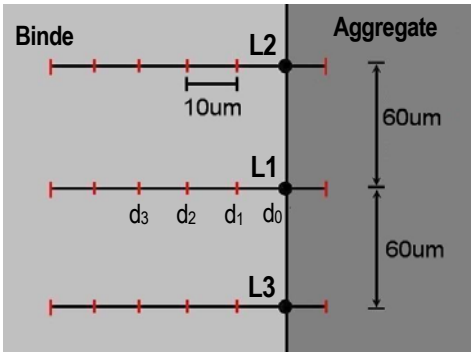

Figure 6: three positions at left observing point

3. Determination of interfacial transition zone

The displacements surrounding left observing point under 0.7 f_c' loading are shown (figure 7), where the negative value of displacement means a contraction in measured plane, vice verse. Displacements in this 170μm region display the binder matrix near the aggregate having different material properties or microstructures. Two turning points discovered at the position away from the surface of aggregate are 80μm and 150μm, respectively. The turning point possibly indicates the boundary of ITZ and the position of a crack. However, this displacement diagram is not enough to determine the range of ITZ yet.

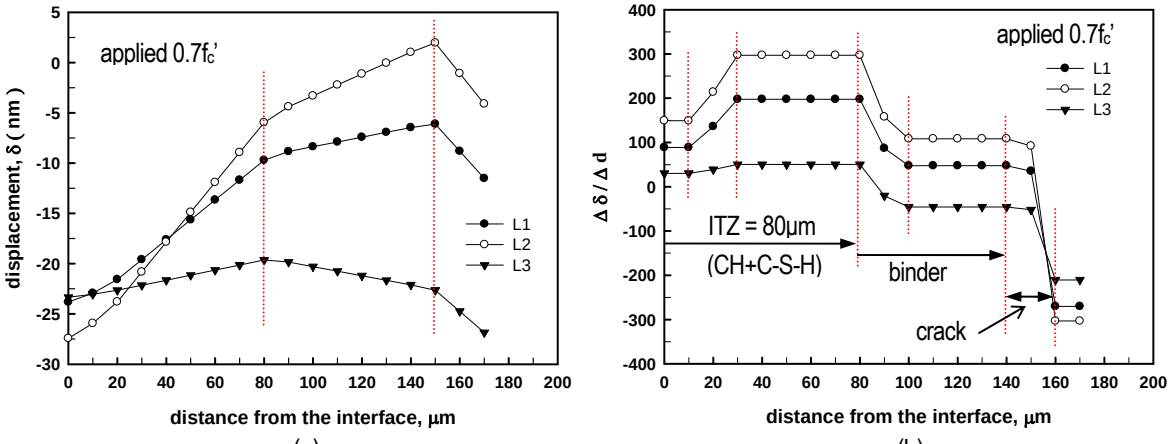

Figure 7: (a) displacement and (b) normalized displacement at left observing point subjected to 0.7f_c'

From the results of displacement (figure 7a), a criterion is proposed to determine ITZ by calculating the differences of displacement between neighboring points with

$$\frac{\Delta\delta}{\Delta d} = \frac{\delta_{i+1} - \delta_i}{d_{i+1} - d_i} \qquad (i = 0, 1, 2, \ldots) \tag{1}$$

where the position at d_0 is just on the aggregate edge (figure 6), d_1 (10μm away from d_0), and sequentially up to d_{17} (170μm away from d_0), and the corresponding displacement at each observing position is denoted as δ_0, δ_1, δ_2, etc. Theoretically, this formula has a constant value as the microstructure of material is homogeneous. Results for displacement-to-distance ratio (normalized displacement) calculated from (1) are shown (figure 7b). There are three displacement transition zones found in 10 ~ 30μm, 80 ~ 100μm and 140 ~ 160μm region.

To look into the material structure of ITZ, we took an image from SEM near L1 position (figure 8). Most crystal structures of calcium hydroxide (CH) and calcium silicate hydrate (C-S-H) occupy a region of 80μm close to the aggregate, and a few CH and C-S-H scatter beyond 80μm region. From the distributions of CH crystal one can determine ITZ [2, 18]. For the zone in 10 ~ 30μm (figure 8), the distributions of CH and C-S-H structure are not uniform. The range of ITZ at L1 point is found at a range of 80μm. Comparisons of figure 7b and figure 8, the values of normalized displacement for L1 point drop tremendously at 80μm and 150μm (figure 7b) representing the boundary of ITZ and the position of a crack respectively. Therefore, we can use the change of normalized displacement near the aggregate to determine the range of ITZ.

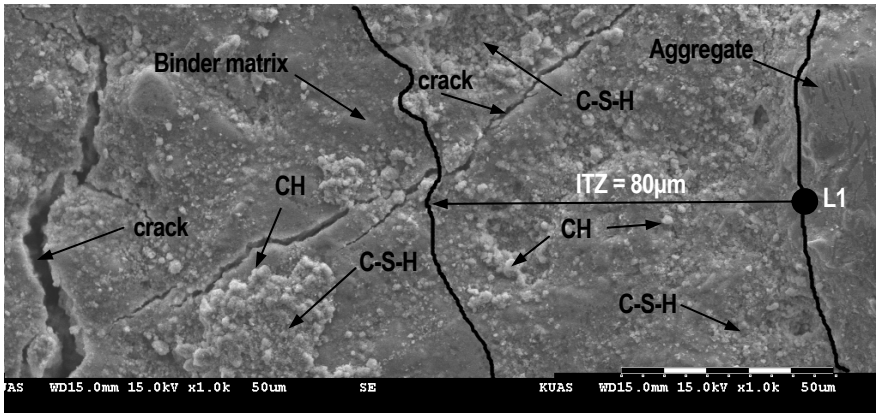

Figure 8: SEM image near L1 position

4. Results and discussion

Dynamic displacements of specimens subjected to a continuous compressive stress from 0 to 0.7 f_c' were monitored at four observing points near the top, bottom, left and right surface of aggregate respectively (figure 2). The displacements were recorded at a range up to 170μm away from the aggregate for each observing point.

At the top observing point, displacements within 170μm region fluctuate according to external loadings (figure 9a). It is hard to find turning points from the displacement diagram except for 0.7 f_c'. To determine the range of ITZ, we use the change of normalized displacements (figure 9b) such that the range of ITZ near the top observing point is about 80μm no matter what loadings were applied. This implies that the applied stress has a less effect in the scope of ITZ before the specimen failed. As the bottom observing point is examined, the measured in-plane displacements also depends on the position away from the edge of aggregate and the loading (figure 10a). The range of ITZ at the bottom is 90μm (figure 10b), a slight larger than at the top.

For the observing points in the lateral of aggregate (L and R point), applied external stresses induce a combination of tension and shear stress to force an early development of microcracks in ITZ. The displacement changes gradually reduce in 0.1 f_c' ~ 0.2 f_c' loading (figure 11a and 12a), due to stress redistributions. The range of ITZ for the left and right side of aggregate was determined at a range of 80μm and 60μm (figure 11b and 12b), in turn. Meanwhile, from the change of normalized displacement, the external loading also shows a less influence to ITZ in both lateral sides of aggregate.

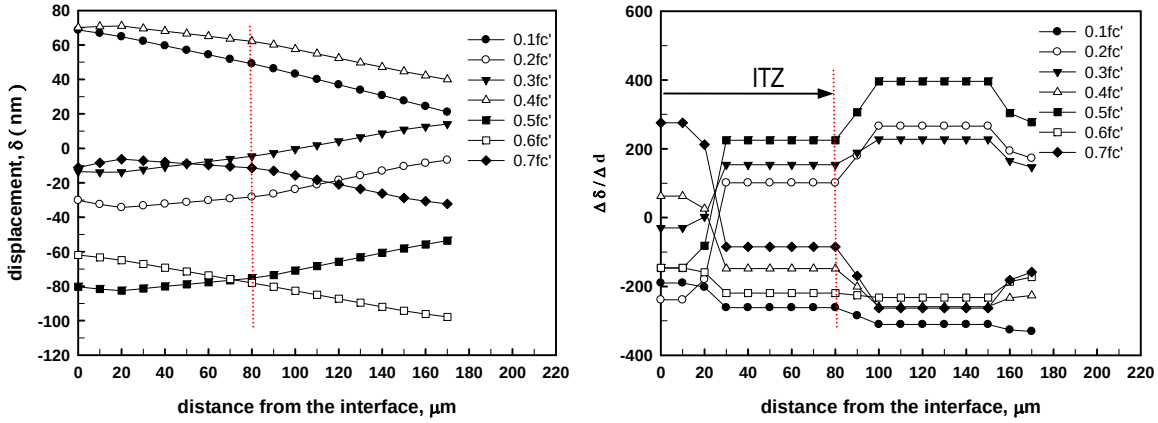

(a) (b)

Figure 9: (a) displacement and (b) normalized displacement at top observing point

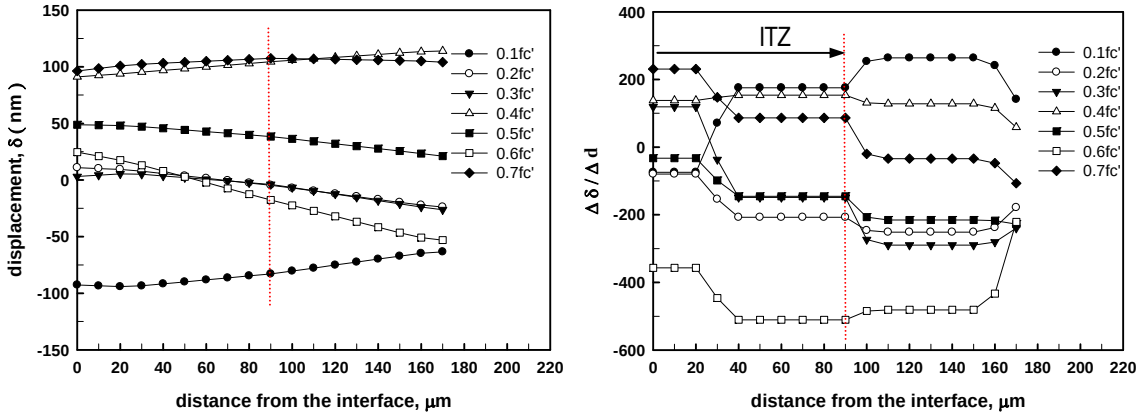

(a) (b)

Figure 10: (a) displacement and (b) normalized displacement at bottom observing point

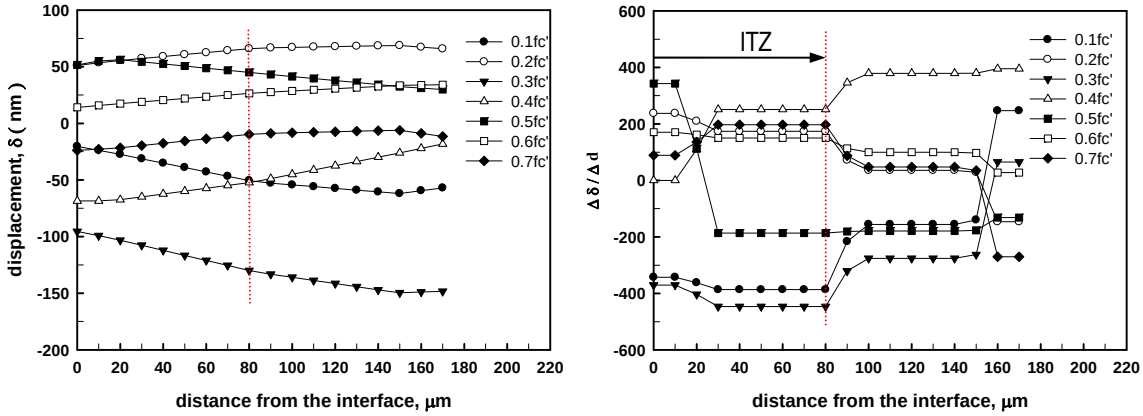

(a) (b)

Figure 11: (a) displacement and (b) normalized displacement at left observing point

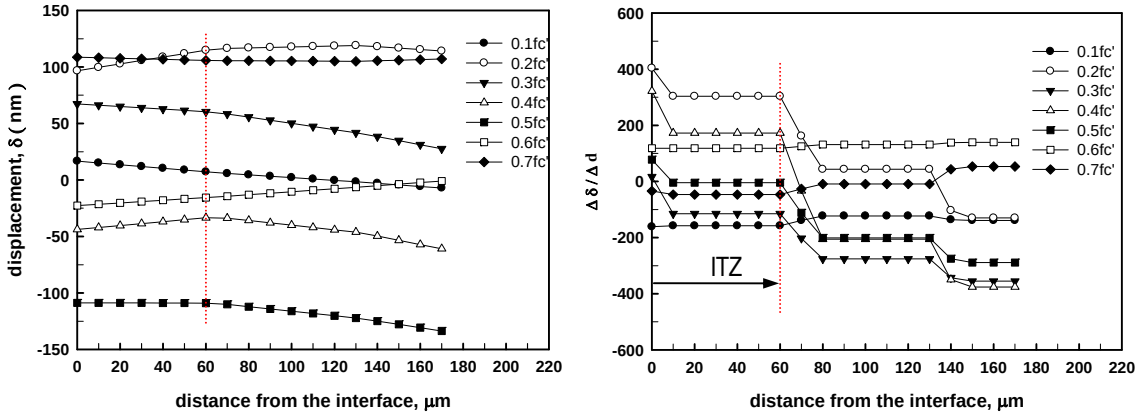

Figure 12: (a) displacement and (b) normalized displacement at right observing point

In general, a stress-strain curve of concrete can be divided into three intervals: first the stress-strain curve is linear within the loading 0 ~ 0.3f_c', then is nonlinear as the loading continue to increase from 0.3 f_c' ~ 0.5 f_c' due to the occurrence of microcracks inside the concrete, and more intense nonlinear behavior induced by the co-linkage of microcracks in 0.5 ~ 0.7f_c' region [19]. From the dynamic displacements measured by ESPI, micro displacements at the bottom observing point with increasing external loadings are shown (figure 13). While the applied stress is within 0.1 f_c' ~ 0.3 f_c', the displacements first increase and then decrease due to microcracks occurring in 0 ~ 90μm region (ITZ). As the applied stress continues to extend till 0.5 f_c', the displacement changes show a reverse behavior caused by new microcracks observed in binder matrix region (beyond 80μm region). At a 0.5 f_c' ~ 0.7 f_c' interval, the trend of displacements is inverse again due to the growing and co-linkage microcracks compared with 0.3 f_c' ~ 0.5 f_c' range. A side effect to interpret the stress-strain relation of cementitious materials is found.

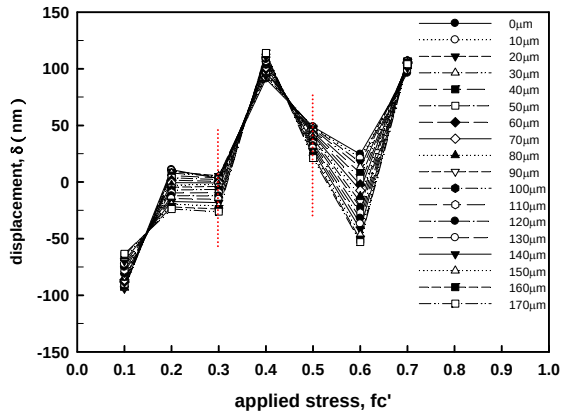

Figure 13: loading effect at bottom observing point

Conclusions

Dynamic displacements were investigated to examine the range of ITZ, with a special reference to the effect of external loading. The judgment of dynamic displacement measured by ESPI has the advantage of understanding the microstructure behavior and mechanical properties without disturbing the original state of the specimen due to applied loading. ESPI method is a substitute measurement to determine ITZ verified by SEM. The applied loading will not affect the determination of ITZ according to ESPI measurement, but the displacement. From the

displacement analysis, ITZ produces microcracks starting at 0.1 f_c', with increasing the quantities of microcracks in 0.2 f_c' ~ 0.4 f_c' range, and binder matrix with some microcracks are found as applied stress reaches 0.4 f_c' ~ 0.6 f_c'. Besides the determination of ITZ, ESPI method is anticipated to evaluate the micromechanical behavior in cementitious materials in future.

Acknowledgments

This study was financially supported by the Taiwan National Science Council under Grant No. NSC 98-2221-E-151-054.

References

[1] Mindess S., "Tests to determine the mechanical properties of the interfacial zone", Interfacial Transition Zone in Concrete, Edited by J.C. Maso, Spon Pre., p. 47-48, 1996

[2] Diamond S., "Considerations in image analysis as applied to investigations of the ITZ in concrete", Cement Concrete Composites, Vol. 23, p.1 71-178, 2001

[3] Liaoa K.Y., Chang P.K., Peng Y.N. and Yang C.C., "A study on characteristics of interfacial transition zone in concrete", Cement Concrete Research, Vol. 34, p. 977-989, 2004

[4] Zhang J., Sun H., Wan J. and Yi Z., "Study on microstructure and mechanical property of interfacial transition zone between limestone aggregate and Sialite paste", Construction Building Materials, Vol. 23, p. 3393-3397, 2009

[5] Diamond S. and Huang J., "The ITZ in concrete-a different view based on image analysis and SEM observations", Cement Concrete Composites, Vol. 23, p. 179-188, 2001

[6] Leemann A., Loser R. and Münch B., "Influence of cement type on ITZ porosity and chloride resistance of self-compacting concrete", Cement Concrete Composites, Vol. 32, p. 116-120, 2010

[7] Elsharief A., Cohen M.D. and Olek J., "Influence of aggregate size, water cement ratio and age on the microstructure of the interfacial transition zone", Cement Concrete Research, Vol. 33, p. 1837–1849, 2003

[8] Leemann A., Münch B., Gasser P. and Holzer L., "Influence of compaction on the interfacial transition zone and the permeability of concrete", Cement Concrete Research, Vol. 36, p. 1425–1433, 2006

[9] Cwirzen A. and Penttala V., "Aggregate–cement paste transition zone properties affecting the salt–frost damage of high-performance concretes", Cement Concrete Research, Vol. 35, , p. 671–679 2005

[10] Gao J.M., Qian C.X., Liu, H. F., Wang, B. and Li, L., "ITZ microstructure of concrete containing GGBS", Cement Concrete Research, Vol. 35, p. 1299-1304, 2005

[11] Ollivier J.P. and Maso J.C. and Bourdette, B., "Interfacial transition zone in concrete", Advanced Cement Based Materials, Vol. 2, p. 30-38, 1995

[12] Zhu W. and Bartos P.J.M., "Application of depth-sensing microindentation testing to study of interfacial transition zone in reinforced concrete", Cement Concrete Research, Vol. 30, p. 1299-1304, 2000

[13] Mouret M., Bascoul A. and Escadeillas G., "Microstructural features of concrete in relation to initial temperature–SEM and ESEM characterization", Cement Concrete Research, Vol. 29, p. 369-375, 1999

[14] Fu Y.F., Wong Y.L., Poon C.S., Tang C.A. and Lin P., "Experimental study of micro/macro crack development and stress–strain relations of cement-based composite materials at elevated temperatures", Cement Concrete Research, Vol. 34, p. 789-797, 2004

[15] Wang X.S., Wu B.S. and Wang Q.Y., "Online SEM investigation of microcrack characteristics of concretes at various temperatures", Cement Concrete Research, Vol. 35, p. 1385-1390, 2005

[16] Kennedy D.M., Schauperl Z. and Greens S., "Application of ESPI-method for strain analysis in thin wall cylinders", Optics and Laser in Engineering, Vol. 41, p. 585-594, 2002

[17] Huang S.J., Lin H.L. and Liu H.W., "Electronic speckle pattern interferometry applied to the displacement measurement of sandwich plates with two fully potted Inserts", Composite Structures, Vol. 79, p. 157-162, 2007
[18] Li Y. and Hu S., "The microstructure of the interfacial transition zone between steel and cement paste", Cement Concrete Research, Vol. 31, p. 385-388, 2001
[19] Mindess S. and Young J. F., “Concrete”, Prentice-Hell, Englewood Cliff, N. J., Chap. 14, 1981.